ChemPubSoc Europe

DOI: 10.1002/celc.201701093

CHEMELECTROCHEM Articles

Some Attributes of Mn^{3+} Sites in Nickel-Based Layered Double Hydroxides during Methanol Electro-oxidation in Alkaline Media

Miguel A. Oliver-Tolentino,[a] Guadalupe Ramos-Sánchez,[b] Arturo Manzo-Robledo,[c] Daniel Ramírez-Rosales,[d] Jorge L. Flores-Moreno,[e] Enrique Lima,[f] and Ariel Guzmán-Vargas*[a]

Ni-based layered double hydroxides (LDHs), or hydrotalcite-like materials (HTs), were synthetized through co-precipitation at constant pH (NiAl and NiMg) and urea hydrolysis (NiMn) methods, and they were tested in the electrochemical methanol oxidation (MOR). The physicochemical properties were explored by using techniques such as X-ray diffraction, FT-IR spectroscopy, as well as electron paramagnetic resonance. In addition, correlation between active site arrangements and electrocatalytic activity was evidenced by density functional calculations. Specific site $\mu(Ni_2Mn\text{-}OH)$ showed the lowest proton energy removal at approximately 3.6 eV and the NiMn LDH sample containing a higher proportion of this site exhibited the best performance for the MOR process, with an enhancement factor of 5.16, which is attributed to limited deactivation of Ni during the reaction. CO_2 production was detected by differential electrochemical mass spectrometry to be on the order of ten times greater than O_2.

1. Introduction

In the context of global environmental problems, triggered from the use of fossil fuels, new electrochemical devices capable to carry out direct transformations of plentiful raw materials into energy, arises as an ecofriendly and cost-effective process. This means the impulse of other sources of energy taking into account the depletion of conventional sources e.g. petroleum, carbon, etc.

Direct methanol fuel cells (DMFCs) are promising alternatives for energy conversion due to their efficiency in power mobile sources for transportation, portable electronics and stationary applications. Meanwhile having a considerable increase in energy efficiency transformation in comparison to traditional heat engines transformations.[1] However, systems as Pt-containing electrodes have not shown large-scale applications for total methanol oxidation reaction (MOR), due to the fact that secondary or parallel reactions such as: oxygen formation, incomplete oxidation and/or other by-products appear during the process; mainly associated to kinetics limitation due to strong adsorption of CO, poisoning the catalytic surface under acid conditions.[2]

Therefore, the use of alkaline electrolytes and electrocatalysts containing non-precious metals are suitable and important alternatives. In this context, Ni-based catalysts have been extensively used in MOR, in specific bimetallic nanostructured catalysts called Ni-M, where M: Cr, Mn, Co and Cu. Thus, diverse materials based on 3d-metal transition, mainly Ni and Co have been studied.[3] Recently, it has been reported that the surface of Ni-based electrodes is poisoned by the strong adsorption of methanol on the active sites, in particular materials containing NiOOH species, thus, one of the main problem is the catalytic deactivation.[4]

In some cases, the strategy is to support active phases as Ni and precious metals on well-structured materials and having large surface area, e.g. graphene oxide. From this approach, interesting performance was showed towards high catalytic

[a] Dr. M. A. Oliver-Tolentino, Dr. A. Guzmán-Vargas
Instituto Politécnico Nacional, ESIQIE-SEPI-DIQI
Laboratorio de Investigación en Materiales Porosos
Catálisis Ambiental y Química Fina (LiMpCaQu-F)
UPALM Edif. 7 P.B. Zacatenco, GAM
México, CDMX 07738, Mexico
E-mail: aguzmanv@ipn.mx
[b] Dr. G. Ramos-Sánchez
CONACYT comisionado a Universidad Autónoma
Metropolitana-Iztapalapa, Departamento de Química
Av. San Rafael Atlixco 186. Col. Vicentina
México, DF 09340, Mexico
[c] Dr. A. Manzo-Robledo
Instituto Politécnico Nacional, ESIQIE-DIQI
Laboratorio de Electroquímica y Corrosión
Edif. Z-5 3er piso, UPALM, Zacatenco, GAM
México, DF 07738, Mexico
[d] Dr. D. Ramírez-Rosales
Instituto Politécnico Nacional
ESFM-Departamento de Física
UPALM Edif. 9 Zacatenco, GAM
México, DF 07738, Mexico
[e] Dr. J. L. Flores-Moreno
Universidad Autónoma Metropolitana-Azcapotzalco
Área de Química de Materiales
Av.SanPablo180, Col. Reynosa Tamaulipas
México, DF 02200, Mexico
[f] Dr. E. Lima
Laboratorio de Fisicoquímica y
Reactividad de Superficies (LaFReS)
IIM – Universidad Nacional Autónoma de México
Circuito Exterior s/n, Cd. Universitaria
Coyoacán, DF 04510, Mexico

activity and stability; although, these systems are complex involving many steps from synthesis and electrode preparation.[2a,b] Based on this, in recent studies lamellar structured materials called Layered Double Hydroxides (LDH) or hydrotalcite-like materials have been reported as electrocatalysts in MOR. Wang et al. demonstrated that NiAl-LDH exhibited higher electrocatalytic activity for methanol oxidation and better stability than $Ni(OH)_2$.[3] Recently an enhancement on electroactivity of Ni^{III}/Ni^{II} redox couple due to substitution of aluminium by iron in LDH, favoring the presence of Ni^{3+} active site was reported by Tonelli's group.[4] Incorporation of sulfur in Co-Ni LDH decreased the charge transfer resistance improving electrocatalytic behavior according to Qian et al.[5]

In order to prepare materials possessing properties for targeting applications, hydrotalcite-like materials have been synthetized by different methods: co-precipitation at high or low supersaturation, urea hydrolysis, sol gel, ion exchange, hydrothermal, among others.[6] Layered structures, similar to brucite layer are formed by the union of blocks containing di and trivalent cations, which are octahedrally coordinated with hydroxyl group. The positive cation charge contribution is balanced by negative charge from anions with different nature and water localized in the region between layers.[7] Composition of brucite-like layer is characterized by $M^{2+}/(M^{2+}+M^{3+})$ ratio commonly called x, the conventional expression for LDHs materials is stated as Equation (1):

$$(M^{2+}{}_{1-x}M^{3+}{}_{x}\ (OH)_2)^{x+}\ [A^{n-}{}_{x/n}]\cdot mH_2O \qquad (1)$$

Thus, this family of materials has the advantage to modify physicochemical properties to be applied in many research fields, e.g. heterogeneous catalysis, adsorption-desorption process, etc.[8]

In this context, the presence of Mn in LDH composition has exhibited interesting electrochemical properties as reported in some studies, i.e. NiMn-LDH materials in energy storage as supercapacitors[9] and; recently as electrocatalyst for water splitting;[10] therefore, the main goal of this work is to propose an approach to explain the influence on electrocatalytic activity of Mn site in NiMn LDH evaluated during methanol oxidation process.

2. Results and Discussion

Di (M2) and trivalent (M1) cation interactions within the layered structure were evaluated by plane wave DFT simulations. The positions of cations were arranged in such manner as shown in Figure 1. This particular configuration has been chosen based on previous analyses, which have indicated that the most probable configuration is in which one trivalent cation (M1) is surrounded by 6 divalent cations (M2) as was reported before.[11,12] Moreover, the spectroscopic characterization later evaluated indicated that this is fairly the configuration found in the synthesized materials.

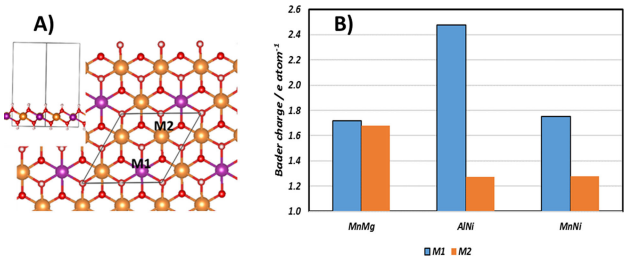

Figure 1. Geometric arrangement of $M1^{3+}$ and $M2^{2+}$ cations in the layer-like sheet of LDH. Red circles: OH, grey lines indicate the unit cell.

2.1. Structural Characterization

Powder X-ray diffraction patterns of the fresh prepared LDHs are presented in Figure 2A, indicating that in all cases, almost

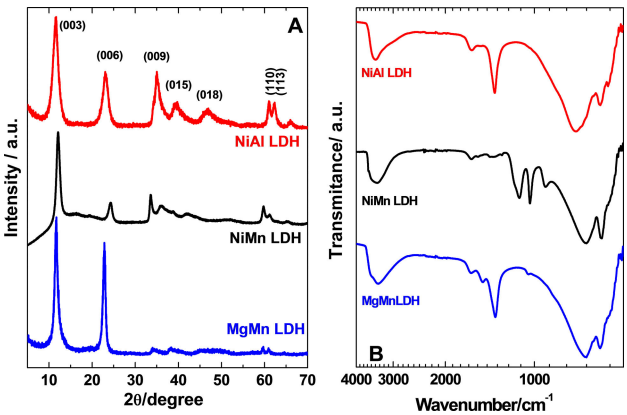

Figure 2. A) X-ray diffraction patterns and B) infrared spectra of LDHs.

pure LDH phase with a good degree of crystallinity was obtained, each sample showed typical XRD profile for LDH compounds characterized by sharp intense peaks according to JCPDS file 22-0700. From (*110*) reflection, *a* lattice parameter ($a=2d_{110}$) can be determined, while *c* parameter was calculated from (*003*) reflection as $c=3d_{003}$.

The lattice parameters shown in Table 1 agree with those reported in literature for similar LDH-CO_3^{2-}-containing MgMn,[13]

Table 1. Lattice parameters of LDHs.

Sample	Lattice parameters (Å)			
	d_{003}	d_{001}	c	a
MgMn LDH	7.551	1.519	22.653	3.039
NiMn LDH	7.308	1.546	21.925	3.092
NiAl LDH	7.589	1.517	22.769	3.034

and NiAl;[14] however, in the case of NiMn LDH, *c* parameter was slightly lower, due to an increase in electrostatic interaction between neighboring layers and interlayer anions.[15] As observed in Table 1 for binary $M^{II}M^{III}$ LDHs, the parameter *a*,

linked to cation-cation distance in Brucite-like layer, increases due to ionic radii of 6-fold coordinated cations (effective ionic radii are: Mn^{2+} = 0.64 Å, Al^{3+} = 0.53 Å, Ni^{2+} = 0.69 Å and Mg^{2+} = 0.72 Å). Thus, for example, *a* parameter for NiMn LDH sample is higher than for NiAl LDH; this situation can be explained in terms of the difference between ionic radii of Mn^{3+} and Al^{3+} cations. A similar trend can be observed for MgMn and NiMn LDH samples.

FTIR spectra of the three LDHs are compared in Figure 2B. For all samples, broad absorption band between 3400 and 3500 cm^{-1} is ascribed to the stretching frequency mode of O–H groups in brucite-like layer and interlaminar water. MgMn and NiAl LDH samples exhibit a band located at 1356 cm^{-1} and 1362 cm^{-1}, respectively, assigned to the ν_3 mode of CO_3^{2-} species in the interlayer region of LDH. This band is absent in NiMn sample indicating that charge-compensating anion is different from CO_3^{2-}. It is worth to mention that NiMn sample was prepared from ammonium persulfate, which acts as oxidizing agent during synthesis, allowing the oxidation of Mn^{2+} to Mn^{3+}.

Redox reaction between $S_2O_8^{2-}$ and Mn^{2+} species forms SO_4^{2-} anions, they can be intercalated into the interlayer region inducing electrostatic interaction with the layers,[16] as was explained in XRD discussion. As a consequence, FTIR spectrum of NiMn LDH (black line in Figure 2B) shows a band centered at 1125 cm^{-1} that is associated to the ν_3 stretching mode of sulfate (free SO_4^{2-} anion shows a band at 1104 cm^{-1} attributed to ν_3 stretching mode[17]). The band observed at 1036 cm^{-1} was attributed to Mn^{3+}-O vibrations. Weak bending modes (ν_2) and symmetric stretching mode (ν_1) were not detected.

Electronic properties of LDHs were explored by UV-Vis and EPR spectroscopy, neither Mg nor Al containing LDHs showed electronic transition under UV-Vis light and EPR analysis conditions. Whereas, for NiAl LDH only one electronic transition associated to Ni^{2+} (t_{2g}^6 e_g^2, S = 1) in octahedral coordination was observed (Figure 3A); with two spin-allowed transition at 643 and 381 nm, and two spin forbidden transitions at 740 and 420 nm.[18] On the other hand, for MgMn LDH only one electronic transition associated to Mn^{3+} (t_{2g}^3 e_g^1, S = 2) in octahedral coordination was presented; with three characteristic bands at ca. 410, 470 and 750 nm,[19] associated to the crystal field d–d transitions. In this context, it is well known that Mn^{3+} exhibits Jahn-Teller distortions, assigned to spin-allowed transition $^5E_{1g} \rightarrow {}^5T_{2g}$ corresponding to one-electron interaction acting near to 500 nm (band ν_{JT}).

MgMn LDH sample showed broad EPR signals around *g* = 2.1060 (Figure 3B, top); which are characteristics of high spin Mn^{2+} (S = 5/2) with exchange and dipolar coupling among them. Line width and EPR profile spectra indicate Mn^{2+}–OH–Mn^{2+} interaction in the layer. This interaction is considered similar to that reported by our group previously,[15] when Fe^{3+} is incorporated instead of Mn^{2+} because both ions are isoelectronic (t_{2g}^3 e_g^2). EPR spectra at room temperature (RT) and 77 K presented interesting differences. MgMn sample showed a broad signal at 300 K (Figure 3B, curve a), but at 77 K this EPR signal decreased (Figure 3B, curve b). This behavior suggests that this sample exhibits ferromagnetic (F) interaction

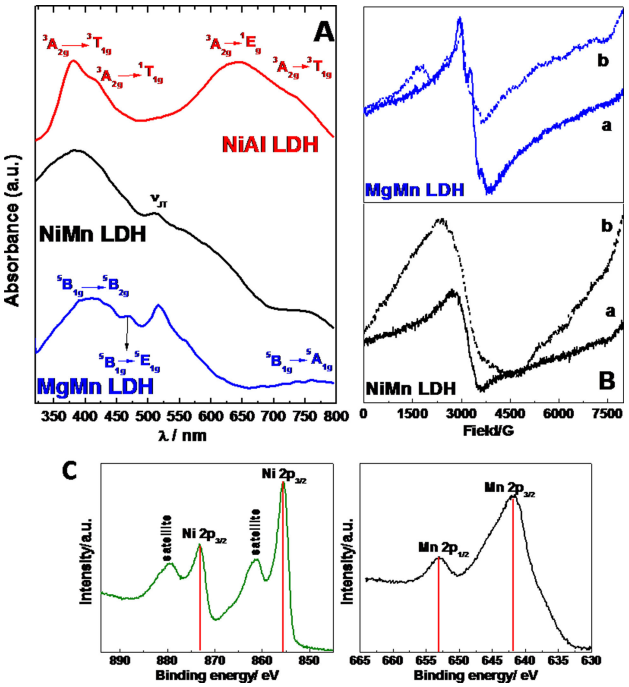

Figure 3. A) UV/Vis-NIR spectra; B) EPR spectra at a) room temperature and b) 77 K; C) XPS spectra of NiMn LDH.

with a small contribution of antiferromagnetic (AF) interaction at RT. However, antiferromagnetic interaction is increased at 77 K.

These EPR results also point out that Mn is present mostly as Mn^{2+}, whereas partial oxidation to Mn^{3+} and/or Mn^{4+} is taking place. Usually, Mn^{3+} is EPR silent owing to its large zero-field splitting.[20] Both Mn^{2+} and Mn^{4+} can give similar EPR spectra. A closer observation reveals any existence of EPR signals which can be assigned to Mn^{4+} species.[19] EPR spectrum at 77 K also shows a broad shoulder around g = 3.86. A similar low-field EPR peak around g = 3.2 was observed in Mn–MCM-41 material,[21] in this case, EPR results were assigned to extra-framework Mn^{2+} cations in distorted tetrahedral symmetry.

In view of our results, it may be reasonable to assume that Mn^{2+} species in MgMn sample be located in distorted octahedral and/or distorted tetrahedral coordination, and there should be more than one Mn^{2+} species.[21]

On the other hand, X- band EPR spectrum of NiMn LDH system in polycrystalline state at room temperature and also at low temperature (77 K), exhibited a single and very broad line with g value around 2.1820 (Figure 3B, bottom). The shape and line width indicate strong dipolar interaction among the spins of Ni and Mn atoms and resulting a ferromagnetic response (F) in the system.[15] Additionally, g value also indicates the highly distorted octahedral system. Such distortion is due to ionic radii of cations and distortions caused by the local crystal field and electron interactions due to Jahn-Teller effect. These electron interactions promote greater electron mobility and consequently an increase in the system conductivity. Thus, It is claimed that oxidation state of Mn is mostly 3+ because those characteristics for Mn^{2+} signals are completely absent (see

spectrum of MgMn LDH sample). Additionally, the oxidation state of Ni and Mn in NiMn LDH was confirmed by X-ray photoelectron spectroscopy (XPS), Figure 3C shows the spectra for Ni and Mn, peaks for Ni $2p_{3/2}$ and $2p_{1/2}$ appear closed to 873.2 and 855.6 eV, respectively, both peaks are accompanied by satellite bands, this indicate the presence of Ni^{2+}. On the other hand, the prominent central peaks associated to Mn $2p_{1/2}$ and $2p_{3/2}$ situated at 652.5 eV and 641.7 eV, respectively, indicate clearly the existence of Mn^{3+}.[10]

2.2. Computational Results

For bulk hydrotalcite-like materials, interlayer region contains charged anions, which made up the charge on hydrotalcite layer like-sheet, thus, one metal donates electrons. In order to represent these changes, the system was optimized removing one electron. For this, Bader charge analysis is a method intended to calculate the electron density enclosed by the atoms, it is based purely on the electronic charge density. Although intuitive it has been used to determine the total charge and the oxidation state of atoms in solids and molecules.[22] In this work, it was used to determine the differences in oxidation states of the cations on the layer surface. By artificially removing one electron and performing Bader analyses we can determine from which atom or group of atoms the charge is preferentially removed. Figure 4A depicts the average charge of M2 (divalent cation) and M1 (trivalent cation), for MnMg LDH system, the Bader charge on both metals is almost the same, thus there will be no specific differentiation among trivalent and divalent cations in the layers, due to that the electron is not specifically removed. On the other hand, on NiAl LDH system Bader charges present huge differences for Al and Ni atoms, consequently the specific reactivity is expected to be different as a result of the higher differences in oxidation states. For MnNi LDH system, there are differences on the cations charge; however, but, the differences are not as extreme as in NiAl LDH system. These results indicate that although the ideal picture of LDH having trivalent and divalent cations has been long accepted, it does not always occur and it is modulated by the specific cations nature, arranging LDH layers.

Decomposition of total Density of States (DOS) on partial DOS provides a method to analyze the participation of specific sites on solid reactivity. Figure 4B presents the differences on partial DOS of three systems near Fermi level. In an initial analysis, the band gap of NiAl LDH is higher than one for NiMn LDH, which might have an effect on its effectiveness as electrocatalysts, since electron transport to the specific reaction site is limited.

Moreover, participation of trivalent cations near to Fermi level is very different on Al and Mn containing LDH. For Mn LDH independently of divalent cation, Mn states arise as the main component of band closer to Fermi level; however, depending on divalent cation, the next band is composed of M^{2+}-O hybridization in the case of NiMn LDH or almost pure oxygen states for MgMn LDH. On the other hand, NiAl LDH is completely different, no Al states are detected close to Fermi level, but only a very small amount of Ni states, thus, participation of Al on redox processes is also very limited.

Superficial hydroxyl groups are active species of LDH,[11] where deprotonation occurs as the first step during electrochemical oxidation. In order to prove the reactivity of layered materials, hydrogen removal energy was calculated for all systems. In this work divalent/trivalent cation ratio was 3, so that the cation arrangement on layer sheet can be one M1

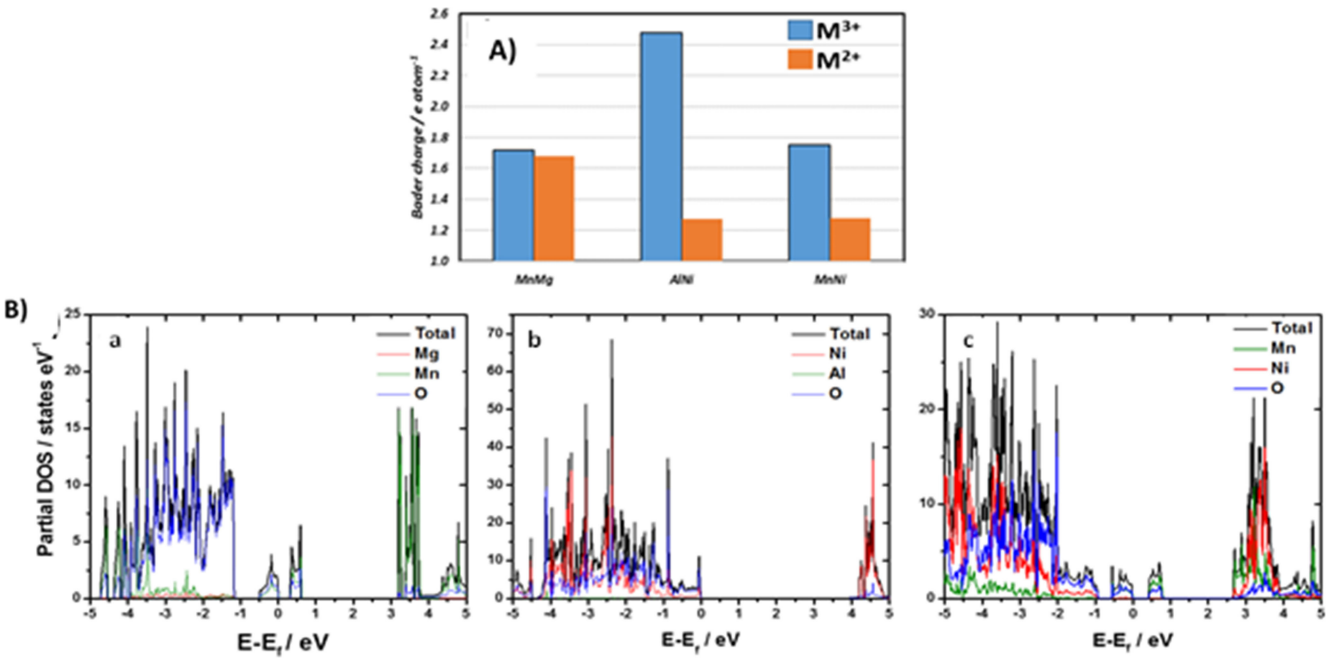

Figure 4. A) Bader metal charge of LDHs: M1 is a divalent and M2 is trivalent cations. B) Partial DOS of LDHs a) MgMn, b) NiAl, and c) NiMn.

cation surrounded by six M2 cations; where the OH is surrounded by three cations producing $\mu(M^{2+}{}_2M^{3+}\text{-OH})$ site; from this, hydrogen removal energy values obtained for this site were in the next order: 5.3 eV > 3.85 eV > 3.64 eV corresponding to configurations $\mu(Ni_2Al\text{-OH})$, $\mu(Mg_2Mn\text{-OH})$ and $\mu(Ni_2Mn\text{-OH})$, respectively, more positive values indicate highly forbidden processes.

This phenomenon can be attributed to Mn^{3+} ability to remove the charge density on oxygen atom in M–O bond, decreasing the effective charge on oxygen in MO–H bond, particularly, on four Mn–O shorter bonds caused by Jahn-Teller distortions,[23] NiAl and NiMn LDH also exhibited the presence of $\mu(Ni_3\text{-OH})$ configuration with 4.7 eV for proton removal as was reported previously.[11]

2.3. Electrochemical Characterization and the Methanol Oxidation Reaction (MOR)

Electrochemical behavior was investigated using cyclic voltammetry (CV) in solution of KOH 1 M at scan rate of 5 mV s^{-1}. The profiles put in clear that in general, electrochemical process is due to insertion/desertion of OH^- ions in the LDH interlayer space, during oxidation/reduction of nickel sites by electron hopping mechanism along the brucite layer structure inducing electroneutrality.[24]

Both Ni based materials exhibited well-defined redox peaks during anodic and cathodic scans (Figure 5), which can be attributed to Ni^{2+}/Ni^{3+} redox couple. NiAl LDH shows a peak at potential of $\Delta E_p = 0.23$ V and formal potential of $E_f = 0.5$ V/SCE; whereas in NiMn LDH, faradic process occurs at lower potential ($E_f = 0.41$ V/SCE) with better electrochemical reversibility ($\Delta E_p = 0.13$ V); indicating that $Mn(OH)_6$ unit plays an important role on electronic properties, this was verified by electrochemical impedance spectroscopy acquired in the middle peak potential (see inset Figure 5). In this case, NiMn LDH exhibits a lower charge transfer resistance than NiAl LDH during oxidation process. The improvement is associated to the electron mobility throughout the layer sheet, which is produced by the presence of Mn^{3+} as it was discussed before in EPR results. This fact is due to that manganese exhibited a band near to Fermi level and their t_{2g} orbitals are partially occupied, promoting the Ni–O hybridization, which decreases the required energy for electron subtraction of Ni^{2+} during the oxidation, as was proposed according to theoretical calculation. Whereas, for MgMn LDH any redox process was exhibited as it is shown in Figure 5; confirming by instance, that only Ni species participate in electrochemical process.

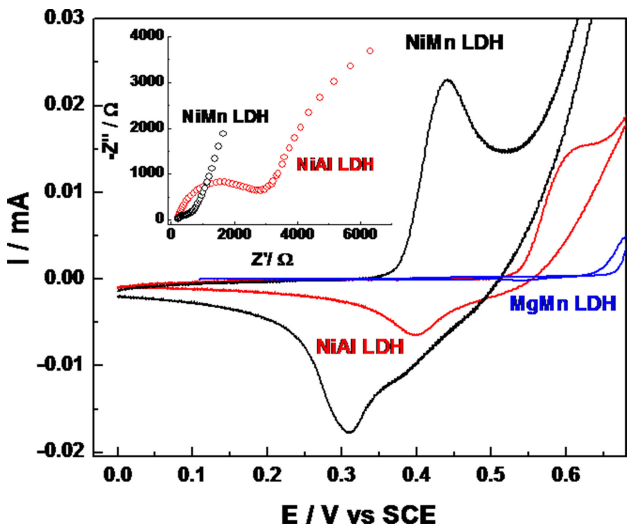

Figure 5. Cyclic voltammetry profiles of LDHs at 5 mV s^{-1} in KOH (1 M); inset: Nyquist plot at applied potential of middle peak potential.

After formation of Ni^{3+} ($t_{2g}^6\ e_g^1$) at $E_{Ni\text{-}onset} = 0.53$ V/SCE during positive-going scan, oxygen evolution reaction (OER) takes place at ca. 0.7 V/SCE in NiAl sample (curve a in Figure 6A). Conversely, methanol oxidation reaction is catalyzed by

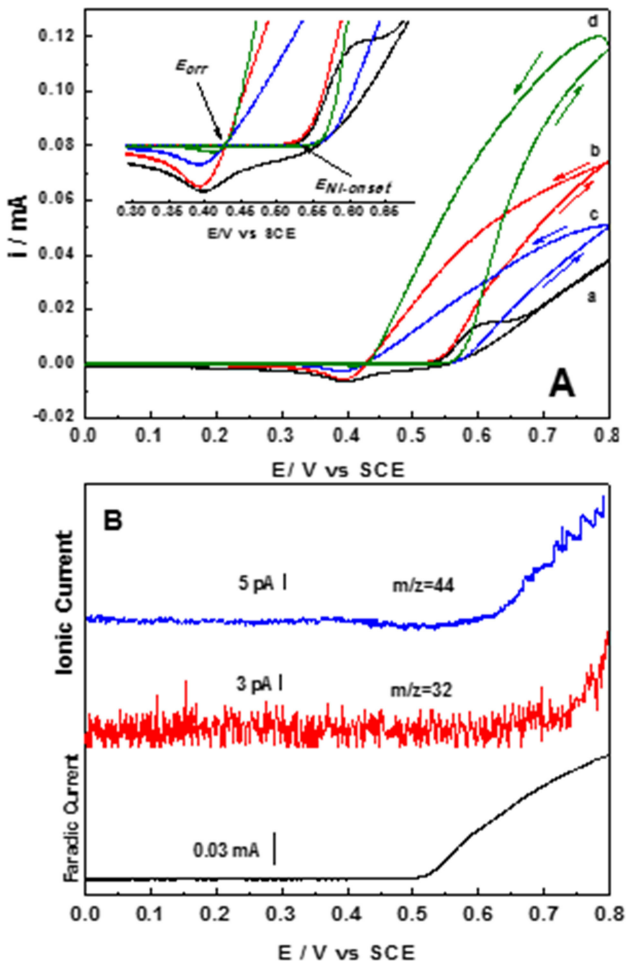

Figure 6. A) Cyclic voltammetry of NiAl LDH in a) KOH (1 M), b) KOH (1 M) + CH_3OH (0.04 M), c) KOH (1 M) + CH_3OH (0.1 M) obtained from methanol addition to experiment without removing the electrode from solution, and d) KOH (1 M) + CH_3OH (0.1 M) with a new electrode surface. B) Current–potential characteristics for NiAl LDH, in 1 M KOH and scan rate of 1 mV s^{-1}, and mass signal profiles obtained using DEMS technique during anodic polarization.

chemical reduction of Ni^{3+} to Ni^{2+}, as can be observed from curve (b) in Figure 6A (initial methanol concentration was 0.04 M). For this case, onset potential is the same as in the case of methanol free solutions; nevertheless the increment in faradic current associated to MOR is more marked, with a crossing potential ca. 0.43 V/SCE suggesting an interfacial modification during positive-going scan (see inset in Figure 6A) as has been observed for electrochemical metallic deposition.[25]

This modification might be associated to the interfacial-adsorbed non-oxidized-methanol in positive-scan direction. Then, as the methanol oxidation rate is much lower than its adsorption rate (Langmuir adsorption),[26] the charge of faradic process related to nickel reduction decreases. As consequence of that, a small portion of Ni^{3+}-sites are available for such oxidation; the calculated EF was 1.73.

Additionally, electrocatalytic stability was studied without removing the electrode from the cell-solution and by adding to initial solution the required amount of methanol to reach 0.1 M. Then, $E_{Ni\text{-}onset}$ shifts to more positive potential (ca. 0.57 V/SCE), see curve (c) in Figure 6A. Moreover, current magnitude linked to MOR is less marked (with calculated $EF \approx 0.5$), as a consequence of adsorbed methanol at the electrode interface, the catalytic activity is inhibited.[27] Increasing the methanol concentration to 0.1 M and using a new electrocatalyst surface, any variation of the onset potential was detected (curve d in Figure 6); however, during applied potential, faradic current increases reaching $EF = 3.43$, confirming that Ni^{+n}-sites are disabled due to methanol adsorption.

Following this analysis, and in order to elucidate the role of Ni-sites and detect the species formed at the electrode-electrolyte interface on MOR and OER; *in situ* differential electrochemical mass spectrometry (DEMS) technique was employed. For such an approach, an alternative electrochemical cell connected to mass spectrometer throughout vacuum system, was used, scan rate was fixed at 1 mV s^{-1}.

For NiAl LDH electrode, during LSV in anodic direction and in 0.04 M of methanol, ionic-current versus potential characteristics indicate the formation of O_2 and CO_2 as final products, as it can be observed from the mass-to-charge ratio $m/z = 32$ and $m/z = 44$, respectively (Figure 6B), not evidence of CO_2 production in absence of methanol was observed indicating that carbon corrosion not occurs, this is in agreement with results reported before.[15]

From Figure 6B, CO_2 production starts at ca. 0.63 V/SCE (after Ni^{3+} is formed); whereas at greater potential than 0.7 V/SCE, the signal associated to oxygen production is evident, suggesting that adsorbed OH^- species on the electrode surface are also oxidized. A closer inspection of these profiles shows ionic-current values for both species in the same order of magnitude (3×10^{-12} and 5×10^{-12} A for oxygen and carbon dioxide, respectively) suggesting an important competition between OER and MOR.

Based on the results obtained from DEMS experiments, one possibility for the general mechanism of oxidation process, is when nickel oxidation starts, promoting deprotonation of μ(Ni_3-OH) site, then, methanol and OH^- adsorption take place; thus, methanol adsorbed is oxidized to CO_2 due to dehydrogenation of α-carbon as has been reported by Casella et al.[28] Whereas, at more anodic potential, adsorbed hydroxyl ions are oxidized to oxygen.

On the other hand, NiMn LDH exhibits lower initial potential for OER (0.64 V/SCE) and the associated-faradic current is higher compared with NiAl LDH sample, (curve a in Figure 7A);

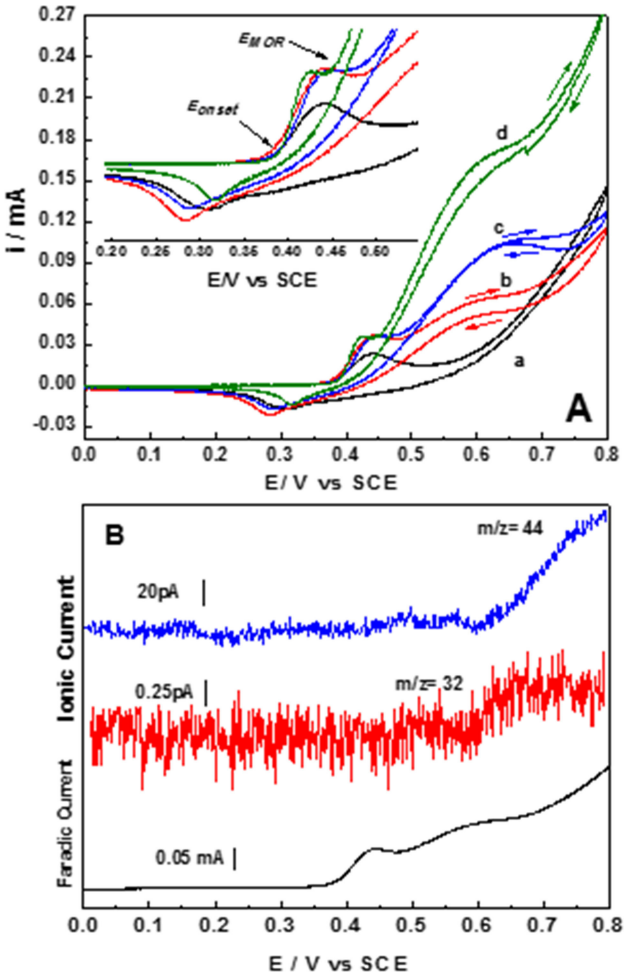

Figure 7. A) Cyclic voltammetry of NiMn LDH in a) KOH (1 M), b) KOH (1 M) + CH_3OH (0.04 M), c) KOH (1 M) + CH_3OH (0.1 M) obtained from methanol addition to experiment without removing the electrode from solution, and d) KOH (1 M) + CH_3OH (0.1 M) with new electrode surface. B) Current–potential characteristics for NiMn LDH, in 1 M KOH and scan rate of 1 mV s^{-1}, and mass signal profiles obtained using DEMS technique during anodic polarization.

indicating better electro-catalytic activity as has been reported elsewhere for other Ni and Mn containing materials,[29] this can be associated to NiMn LDH exhibiting better electron mobility on the layer sheet as was discussed in EPR results. Whereas in presence of methanol solution of 0.04 and 0.1 M, the current attributed to nickel oxidation increases (see inset), and the weak peak attributed to MOR is observed at ca. 0.57 V/SCE, followed by slope modification associated to evolution of oxygen. Calculated *EF* for methanol concentration of 0.04 M was 2.35 (curve b).

The addition of methanol (*in-situ*) increasing solution concentration until 0.1 M, showed an increment in methanol oxidation current (curve c in Figure 7A), electrocatalytic activity was increased considerably obtaining the $EF = 5.16$, indicating that catalyst deactivation is limited or controlled, this fact was verified by electrochemical oxidation of methanol (0.1 M) using new electrocatalyst surface (curve d), in that experiment current associated to MOR was clearly increased. At these conditions, current for OER decreases as methanol concentration increases.

Interestingly, within experimental error, at the same onset potential (0.6 V/SCE), ionic current for CO_2 is in the order of magnitude of 10 times greater than ionic current for O_2, see Figure 7B. Suggesting that MOR and OER occur simultaneously on different electrocatalytic sites; so that methanol can be absorbed preferentially on μ(Ni_2Mn-OH) site type by interaction of non-bonded electron pairs of oxygen from CH_3-O with partially vacant *d*-orbital of Mn species,[30] whereas OH^- adsorption is favored on μ(Ni_3-OH) site, which inhibits the oxygen production, due to μ(Ni_2Mn-OH) site shows lower energy proton removal, therefore, this last site acts as methanol attractor protecting the μ(Ni_3-OH) site; thus, methanol will be faster and preferentially adsorbed, reacting before that the OH^- species reach the same site (μ(Ni_3-OH)).

Electrocatalytic stability on methanol oxidation of LDH's was evaluated by chronoamperometric experiments at 0.6 V vs SCE during 3500 s (Figure 8), it is evident that NiMn LDH

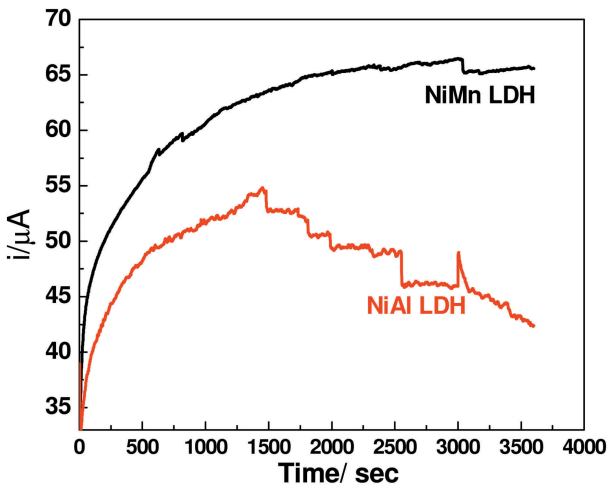

Figure 8. Chronoamperometric performance at 0.6 V vs SCE of LDHs in KOH (1 M) + CH_3OH (0.1 M).

showed higher current than NiAl LDH, further, the oxidation current for NiAl LDH decrease after 1500 s, whereas the current for NiMn LDH is stable and constant; this result confirms the stability of octahedral Mn^{3+} in LDH structure during oxidation process, which contributes to the inhibition of nickel poisoning.

3. Conclusions

A series of Ni containing layered hydroxides were prepared and evaluated on electrochemical methanol oxidation. The results clearly showed that the presence of manganese in NiMn LDH improves the electrocatalytic properties associated to nickel, it was mainly associated to specific Mn site which; showed lowest deprotonation energy associated to high electron mobility trough the brucite-type layer. Ionic current for CO_2 was in the order of 10 times greater than for O_2, this is an evidence of MOR and OER occur simultaneously on different electrocatalytic sites; methanol is absorbed preferentially on μ(Ni_2Mn-OH) site type by interaction of non-bonded electron pairs of oxygen from methanol; thus, catalytic deactivation is partially inhibited.

Experimental Section

Materials Preparation

NiAl LDH was prepared through high saturation co-precipitation method, briefly 0.117 mol of NaOH and 0.034 mol of Na_2CO_3 were dissolved in 100 mL of deionized water; pH of this solution was 13.4. A second solution was prepared by dissolving 0.034 mol of $Ni(NO_3)_2 \cdot 6H_2O$ and 0.017 mol of $Al(NO_3)_3 \cdot 9H_2O$ in 100 mL of deionized water. While maintaining the first solution under vigorous stirring, the second solution was slowly added by means of a peristaltic pump. After complete addition, the resultant slurry was stirred for 2 h at room temperature; pH of the suspension was 9.5. Finally, the suspension was stirred for 2 days at 50 °C, and then the solid obtained was separated by centrifugation, rinsed thoroughly with warm distilled water, and dried overnight at 80 °C.

NiMn LDH material was synthetized by urea hydrolysis method with slight variations.[11b] Ammonium persulfate was used to oxidize Mn^{2+} to Mn^{3+} ions during synthesis. Nickel nitrate hexahydrate, $Ni(NO_3)_2 \cdot 6H_2O$, manganese nitrate tetrahydrate, $Mn(NO_3)_2 \cdot 4H_2O$, and urea, NH_2CONH_2, were dissolved in 100 mL of distilled water at room temperature, molar ratio was Ni:Mn:urea = 4:1:7. The solution was transferred into a 300 mL Teflon-lined Parr reactor and heated at 180 °C for 48 h. The product was filtered, washed several times with distilled water, and finally dried overnight at 100 °C.

On the other hand, MgMn LDH material containing carbonate ions was prepared by conventional co-precipitation method under high supersaturation conditions.[14] A solution 0.04 M of Mg^{2+} and Mn^{2+} was prepared by dissolving magnesium chloride hexahydrate ($MgCl_2 \cdot 6H_2O$) and manganese chloride tetrahydrate ($MnCl_2 \cdot 4H_2O$) in 100 mL of distilled water. Molar ratio Mg^{2+}/Mn^{2+} was fixed at 3. Separately, solution with 100 mL of NaOH 0.2 M and Na_2CO_3 0.1 M was prepared. This solution was added drop wise to the solution containing Mg^{2+} and Mn^{2+} at rate of 2 mL/min. At the end of addition, a suspension was obtained and aged at room temperature overnight. Then, it was filtered; solids were washed several times with distilled water, and finally dried at 100 °C.

Electrode Preparation

Modified carbon paste electrodes (MCPE) were prepared by mixing graphite powder (Alfa Aesar, 99.9995 %), silicon oil (Aldrich), and the corresponding LDH at 20 %wt. The mixture was mechanically homogenized and inserted in a 2 mm diameter cylinder (0.0314 cm^2). Electrode surface contact was made with Pt wire.

Physical Characterization

Structural characterization of LDHs by X-ray diffraction (XRD) was performed on a Philips X'PERT PRO instrument using Cu Kα1 radiation (λ = 1.542 Å, 45 kV, and 40 mA); whereas IR analyses were recorded with a Fourier transform infrared (FT-IR) spectrophotometer PerkinElmer FRONTIER equipped with an attenuated total reflectance accessory (ATR).

Electronic properties were studied with an UV-Vis-NIR spectrophotometer PerkinElmer Lambda 950. EPR spectra were recorded on an X-band Bruker EPR ELEXSYS II E500 operating at 9.44 GHz. A modulation field of 10 G and a frequency of 100 KHz were applied. The first derivative of power adsorption was detected as a function of applied field, and the field range was 0–8000 G. X-ray photoelectron spectroscopy (XPS) was carried out using a K-alpha Thermo Fischer Scientific spectrometer with a monochromatic AlKα radiation (1487 eV) as an X-Ray source and was micro-focused at the source to give a spot size on the sample of 400 μm in diameter. XPS survey and high-resolution spectra were collected using analyzer pass energies of 160 and 40 eV, respectively. In order to compensate effects related to charge shift, O1s peak at 531.0 eV was used as internal standard. The samples remained in the prechamber for 15 h and were later transferred to the analytical chamber with a base pressure of 1×10^{-9} Torr.

DFT Simulations

The layer system showed in Figure 1 was relaxed until the forces between atoms were lower than 0.05 eV/Å. Plane wave expansion was optimized to 600 eV and Brillouin zone was sampled following Monkhorst-Pack 13×13×1 gamma centered meshes. Perdew-Burke-Ernzerhof (PBE) exchange-correlation functional was utilized in addition to GGA + U Dudarev approach to calculate high electronic correlation of system. The optimal effective Hubbard (U_{eff}) parameter was used in all simulations, U_{eff} values for Al, Mn, Ni were directly taken from those reported in literature Ni = 6.0, Mn = 3.9, Al and Mg = 0. Bader charge analyses and partial density of states (DOS) were calculated as well as hydrogen removal energy for the systems under study.

Electrochemical Experiments

Electrochemical analyses were carried out at room temperature on a potentiostat – galvanostat VERSASTAT3-400 (Princeton Applied Research). A three-electrode standard electrochemical cell was used for cyclic voltammetry (CV) measurements at 5 mV s^{-1}, with a carbon rod as counter electrode and saturated calomel electrode (SCE) as reference. For the experiments, carried out by triplicate, working electrode was made from LDH synthesized materials, immersed in carbon paste electrode (CPE) matrix prepared as was described above, electrolyte support was KOH solution (1 M) and two solutions with different methanol concentrations 0.04 M and 0.1 M, applied potential was from 0 to 0.8 V/SCE. In order to quantify electrocatalytic activity toward methanol electro-oxidation, enhancement factor (*EF*) was calculated using Equation (2).[31]

$$EF = \frac{I_{MetOH} - I_{OH}}{I_{OH}} \quad (2)$$

Where I_{MetOH} and I_{OH} are current intensity at 0.6 V/SCE in presence and absence of methanol, respectively.

For *in situ* experiments during polarization, DEMS coupled with a homemade electrochemical cell made of Teka-Peek was used; experimental details have been reported in previous work.[14]

Acknowledgements

Authors thank CONACYT INFR-2014-225161, CONACYT 225115 INFR-2014-01, PAPIIT-IN106517 and SIP 20170776. A.G.-V. thanks LaFReS-IIM-UNAM for the sabbatical stay during which this work was carried out.

Conflict of Interest

The authors declare no conflict of interest.

Keywords: Methanol Oxidation · Jahn-Teller distortions · electron mobility · catalytic deactivation · deprotonation energy

[1] A. B. Soliman, H. S. Abdel-Samad, S. S. Abdel Rehim, M. A. Ahmed, H. H. Hassan, *J. Power Sources* **2016**, *325*, 653–663.
[2] a) W. Huang, H. Wang, J. Zhou, J. Wang, P. N. Duchesne, D. Muir, P. Zhang, N. Han, F. Zhao, M. Zeng, J. Zhong, C. Jin, Y. Li, S.-T. Lee, H. Dai, *Nature Comm* **2015**, *6*, 10035; b) X. Du, C. Du, P. Cai, W. Luo, G. Cheng, *ChemCatChem* **2016**, *8*, 1410–1416; c) L. Preda, T. Kondo, T. Spataru, M. Marin, M. Radu, P. Osiceanu, A. Fujishima, N. Spataru, *ChemElectroChem* **2017**, *4*, 1908–1915; d) P. Wang, T. Kottakkat, M. Bron, *ChemElectroChem* **2015**, *2*, 1396–1402.
[3] Y. Wang, D. Zhang, W. Peng, L. Liu, M. Li, *Electrochim. Acta* **2011**, *56*, 5754–5758.
[4] Y. Vlamidis, S. Fiorilli, M. Giorgetti, I. Gualandi, E. Scavetta, D. Tonelli, *RSC Adv.* **2016**, *6*, 110976–110985.
[5] L. Qian, W. Chen, M. Liu, Q. Jia, D. Xiao, *ChemElectroChem* **2016**, *3*, 950–958.
[6] J. He, M. Wei, B. Li, Y. Kang, D. G. Evans, X. Duan, *Preparation of Layered Double Hydroxides* in Layered Double Hydroxides (Eds.: X. Duan, D. G. Evans), Springer, Berlin Heidelberg, **2006**, pp. 89–119.
[7] D. Zhou, Z. Cai, Y. Bi, W. Tian, M. Luo, Q. Zhang, Q. Zhang, Q. Xie, J. Wang, Y. Li, Y. Kuang, X. Duan, M. Bajdich, S. Siahrostami, X. Sun, *Nano Res.* **2017**.
[8] a) M. J. Martínez-Ortiz, M. A. de la Rosa-Guzmán, J. R. Vargas-García, J. L. Flores-Moreno, N. Castillo, A. Guzmán-Vargas, S. Morandi, R. M. Pérez-Gutiérrez, *The Canadian Journal of Chemical Engineering*, In press, DOI; 10.1002/cjce.22946; b) A. Guzmán-Vargas, E. Lima, G. A. Uriostegui-Ortega, M. A. Oliver-Tolentino, E. E. Rodríguez, *Appl. Surf. Sci.* **2016**, *363*, 372–380; c) R. Xie, G. Fan, L. Yang, F. Li, *ChemCatChem* **2016**, *8*, 363–371; d) T. Wen, X. Wu, X. Tan, X. Wang, A. Xu, *ACS Appl. Mater. Interfaces* **2013**, *5*, 3304–3311.
[9] a) X. L. Guo, X. Y. Liu, X. D. Hao, S. J. Zhu, F. Dong, Z. Q. Wen, Y. X. Zhang, *Electrochim. Acta* **2016**, *194*, 179–186; b) W. Quan, Z. L. Tang, S. T. Wang, Y. Hong, Z. T. Zhang, *Chem. Commun.* **2016**, *52*, 3694–3696; c) H. Sim, C. Jo, T. Yu, E. Lim, S. Yoon, J. H. Lee, J. Yoo, J. Lee, B. Lim, *Chemistry – A European Journal* **2014**, *20*, 14880–14884.
[10] W. Ma, R. Ma, J. Wu, P. Sun, X. Liu, K. Zhou, T. Sasaki, *Nanoscale* **2016**, *8*, 10425–10432.
[11] A. Guzmán-Vargas, J. Vazquez-Samperio, M. A. Oliver-Tolentino, G. Ramos-Sánchez, J. L. Flores-Moreno, E. Reguera, *Electrocatalysis* **2017**, *8*, 383–391.
[12] P. J. Sideris, U. G. Nielsen, Z. Gan, C. P. Grey, *Science* **2008**, *321*, 113–117
[13] X. Chang, X. Zhang, N. Chen, K. Wang, L. Kang, Z.-H. Liu, *Mater. Res. Bull.* **2011**, *46*, 1843–1847.
[14] R. Chitrakar, S. Tezuka, A. Sonoda, K. Sakane, K. Ooi, T. Hirotsu, *J. Colloid Interface Sci.* **2005**, *290*, 45–51.
[15] M. A. Oliver-Tolentino, J. Vázquez-Samperio, A. Manzo-Robledo, R. d. G. González-Huerta, J. L. Flores-Moreno, D. Ramírez-Rosales, A. Guzmán-Vargas, *J. Phys. Chem. C* **2014**, *118*, 22432–22438.

[16] C. Barriga, J. M. Fernández, M. A. Ulibarri, F. M. Labajos, V. Rives, *J. Solid State Chem.* **1996**, *124*, 205–213.
[17] a) Z. Liu, R. Ma, Y. Ebina, N. Iyi, K. Takada, T. Sasaki, *Langmuir* **2007**, *23*, 861–867; b) G. A. Caravaggio, C. Detellier, Z. Wronski, *J. Mater. Chem.* **2001**, *11*, 912–921.
[18] A. I. Lapshin, K. A. Tleulieva, *J. Appl. Spectrosc.* **1976**, *24*, 484–487.
[19] S. Velu, N. Shah, T. M. Jyothi, S. Sivasanker, *Microporous Mesoporous Mater.* **1999**, *33*, 61–75.
[20] D. Zhao, D. Goldfarb, *J. Chem. Soc. Chem. Commun.* **1995**, 875–876.
[21] J. Xu, Z. Luan, T. Wasowicz, L. Kevan, *Microporous Mesoporous Mater.* **1998**, *22*, 179–191.
[22] G. Henkelman, A. Arnaldsson, H. Jónsson, *Comput. Mater. Sci.* **2006**, *36*, 354–360.
[23] S. Hirai, S. Yagi, A. Seno, M. Fujioka, T. Ohno, T. Matsuda, *RSC Adv.* **2016**, *6*, 2019–2023.
[24] E. Scavetta, M. Berrettoni, M. Giorgetti, D. Tonelli, *Electrochim. Acta* **2002**, *47*, 2451–2461.
[25] M. A. Oliver-Tolentino, A. Guzmán-Vargas, E. M. Arce-Estrada, D. Ramírez-Rosales, A. Manzo-Robledo, E. Lima, *J. Electroanal. Chem.* **2013**, *692*, 31–39.
[26] M. S. Ureta-Zañartu, A. Alarcón, G. Muñoz, C. Gutiérrez, *Electrochim. Acta* **2007**, *52*, 7857–7864.
[27] D. Chen, S. D. Minteer, *J. Power Sources* **2015**, *284*, 27–37.
[28] I. G. Casella, T. R. I. Cataldi, A. M. Salvi, E. Desimoni, *Anal. Chem.* **1993**, *65*, 3143–3150.
[29] a) O. Aaboubi, A.-Y. Ali-Omar, E. Dzoyem, J. Marthe, M. Boudifa, *J. Power Sources* **2014**, *269*, 597–607; b) I. Danaee, M. Jafarian, A. Mirzapoor, F. Gobal, M. G. Mahjani, *Electrochim. Acta* **2010**, *55*, 2093–2100.
[30] R. M. A. Hameed, *Appl. Surf. Sci.* **2015**, *357*, 417–428.
[31] A. Guzmán-Vargas, M. A. Oliver-Tolentino, E. Lima, J. Flores-Moreno, *Electrochim. Acta* **2013**, *108*, 583–590.

Manuscript received: October 14, 2017
Version of record online: December 19, 2017